Rigorous electromagnetic analysis of dipole emission in periodically corrugated layers: the grating-assisted resonant-cavity light-emitting diode

Danaë Delbeke, Peter Bienstman, Ronny Bockstaele, and Roel Baets

Department of Information Technology, Ghent University, Sint-Pietersnieuwstraat 41, B-9000 Gent, Belgium

Received July 2, 2001; revised manuscript received October 11, 2001; accepted October 18, 2001

We study the grating-assisted light-emitting diode, an LED design for high brightness based on a resonant cavity containing one- or two-dimensionally periodically corrugated layers (grating). We give in detail a generally applicable electromagnetic analysis based on the rigorous coupled-wave theory to calculate the extraction efficiency of spontaneous emission in a periodically corrugated layer structure. This general model is then specified on the grating-assisted resonant-cavity LED, showing simulated efficiencies of more than 40%.

OCIS codes: 050.1950, 050.2230, 230.3670.

1. INTRODUCTION

The increasing use of solid-state light sources in commercial applications such as automobile lighting, displays, and optical interconnects, stimulates the research on high-brightness, highly efficient light emitters. Semiconductor LEDs, mostly showing internal quantum efficiencies close to 100% and having a simple, robust structure and a long lifetime, are considered to be suitable candidates for these applications. Ordinary semiconductor LEDs, however, show an overall efficiency of only a few percent. The external quantum efficiency is limited by total internal reflection at the semiconductor–air interface (e.g., critical angle θ_c for total internal reflection at a GaAs–air interface is only 16°).

Several advanced structures and techniques that enhance the efficiency of the LED have been proposed. The critical angle θ_c can be increased by embedding the LED in a transparent epoxy dome with high refractive index. If the dome is curved and sufficiently large, all light will hit the epoxy–air interface within the critical angle.[1] Alternatively, the light can be extracted from multiple output planes.[1] Other techniques alter the path of the photon inside the semiconductor until it reaches the semiconductor–air interface within the extraction cone. This can be done in a controlled way, such as use of LEDs with a radial outcoupling taper,[2] truncated-inverted-pyramid LEDs,[3] or in a more randomized way, such as use of surface-roughened non-resonant-cavity LEDs (NRCLEDs).[4] The latter achieves overall efficiencies of 46% by redistributing the light at the roughened surface on top of the active region and around the mesa.[5]

In a resonant-cavity LED (RCLED), the spontaneous emission is generated in a Fabry–Perot resonator, in which interference effects alter the internal angular power distribution.[6,7] The preferential propagation direction of the photons can be forced toward the extraction cone. This increase of directivity and/or efficiency due to redistribution of the photons must be distinguished from the case of enhancement of spontaneous emission rate by the Purcell factor $(3Q/4\pi^2)(\lambda^3/V)$, defined for three-dimensional optical cavities of volume V and mode quality factor $Q = \Delta\lambda/\lambda$, with $\Delta\lambda$ the narrow emission linewidth $\Delta\lambda$ around λ, where Q is the smallest quality factor, or $\Delta\lambda/\lambda$.[6] Because of the rather small reflectivity coefficients of the cavity mirror(s) in most cases, the Purcell factor tends to 1, resulting in a neglectable enhancement of spontaneous emission rate. Over the past few years, research on RCLEDs using an electrically pumped $p-n$ diode placed between a metallic mirror/electrical contact and a distributed Bragg reflector (DBR) has resulted in devices with overall quantum efficiencies of 26%.[8] However, again, only the resonant power emitted in a limited numerical aperture around the direction perpendicular to the substrate, corresponding to the critical angle θ_c, can be extracted. The optical power coupled to the so-called leaky DBR modes, which are totally internally reflected at the semiconductor–air interface and to the laterally propagating or guided modes, which are totally internally reflected at the DBR mirror, is lost (except through partial photon recycling by reabsorption[9]). These losses cause the external extraction efficiency to be substantially lower than 100%.

A solution to this loss of power in the unextractable guided modes can be found in a two-dimensional (2D)-periodic wavelength-scaled grating integrated into one or more of the interfaces of the resonant cavity. Several design approaches can be distinguished. The periodic corrugation can provide a bandgap in the dispersion relation of the guided modes at the frequency of emission. Emission will then initially be prevented in the guided modes.[10] Textured metallic mirrors in thin-film resonant cavities providing a bandgap for the TM_{-1} coupled surface-plasmon polariton mode[11] and the lowest-order

TE mode[12] have been demonstrated. Alternatively, the grating can be used for purely optical photon recycling. The diffractive properties of the periodic grating can redirect the laterally propagating resonant guided mode to an extractable direction in the extraction cone. Because of the high power fraction in these guided modes, the use of such gratings will then result in a higher external extraction efficiency. We will hereafter call these devices grating-assisted RCLEDs (GA-RCLEDs), which are the subject of this paper. GA-RCLEDs have been studied in the form of thin-film devices that have a periodically corrugated mirror,[13] and they have been developed in the form of thin films with a periodic wavelength-scale structure in the optically active layer[14] and in the form of asymmetric cavities with a DBR mirror and a metallic mirror[15] or a DBR and a semiconductor–air interface.[16] A variation on the latter can be found in a 2D periodic corrugation surrounding the active region. In these devices, the Fabry–Perot mode is extracted in the central part of the light source where the layers are homogeneous, and the guided mode leaves the semiconductor in the surrounding periodically corrugated region.[17,18]

This paper presents a model for spontaneous emission in periodically corrugated layer structures. The proposed analysis is equivalent to the one proposed by Rigneault *et al.*[19] but differs in that it includes the dependence of the electric field in the cavity on dipole position in relation to the periodic unit cell defined by the Bragg vectors (Subsection 3.D). The electromagnetic analysis presented is applicable for any one-dimensional (1D) or 2D periodically corrugated layer structure. The examples and simulations presented are restricted to GA-RCLEDs at 980 nm in form of a bottom-emitting asymmetric RCLED that has a bottom DBR mirror and a periodic corrugation in the metallic top interface to diffract the guided mode to the extraction cone. The grating coincides with the active region. The metallic interface will act both as diffractive mirror and as electrical contact. These devices have straightforward processing and show an increasing production yield.

The paper is structured as follows: In Section 2 the device concept is highlighted in greater detail. The section is therefore subdivided into three parts corresponding to the basic issues of a GA-RCLED: (A) spontaneous emission in layered structures, (B) extraction of in-plane propagating waves by means of a grating in passive waveguides, and (C) the combination of (A) and (B). Section 3 describes the electromagnetic analysis on which the numerical calculations used to simulate dipole emission inside periodically corrugated layer structures are based. Numerical results for GA-RCLEDs with a 1D or a 2D grating as cavity mirror are presented in Section 4; Section 5 concludes the paper.

2. CONCEPT OF A GRATING-ASSISTED RESONANT-CAVITY LED

A. Dipole Emission in a Planar Cavity

The angular distribution of spontaneous emission in bulk semiconductors can often be regarded as isotropic. However, when the emitting dipole is placed inside a cavity, photons can be redistributed by means of interferences.[6,7] Four ways can be distinguished in which the photons are redistributed: (1) outside modes, (2) guided modes, (3) leaky modes, and (4) metal absorption in the case in which a metallic mirror is used. The outside modes or Fabry–Perot modes with $k_{\parallel} < \omega n_{\mathrm{sur}}/c = k_c$ (n_{sur} is the refractive index of the surrounding material, and $k_{\parallel} = k_{xy}$ is the wave-vector component lying in the plane of the multilayer structure) can be extracted [Fig. 1(a)]. This extraction causes the typically low Q factor of these modes. The guided modes, in contrast, are trapped in the cavity because of total internal reflection (TIR) at the mirror interfaces $\{k_{\mathrm{TIR}}^{\mathrm{mir1}}, k_{\mathrm{TIR}}^{\mathrm{mir2}}\}_{\max} < k_{\parallel}$. They show unity round-trip conditions for the complex field amplitude in the absence of damping and consequently a higher Q factor. When a DBR mirror is used, these guided modes can couple evanescently to the outside medium. In this case they are rather referred to as "quasi"-guided modes. The third channel for redistribution was referred to as leaky modes: photons "leak" through the DBR mirror when $k_c < k_{\parallel} < \{k_{\mathrm{TIR}}^{\mathrm{mir1}}, k_{\mathrm{TIR}}^{\mathrm{mir2}}\}_{\max}$ and are absorbed in the substrate, as they total internally reflect at the substrate–vacuum interface. Guided modes, leaky modes, and metal absorption cause the external extraction efficiency to be substantially lower than 100%.

The distribution of the photons over the four channels depends strongly on the design of the cavity. An initial distinction has to be made regarding whether a DBR mirror is used in the cavity. Thin-film devices without a DBR mirror do not support leaky modes. The emitted power can be efficiently concentrated in a unique guided mode when the thin film is adequately designed. Cavities with a DBR mirror, in contrast, do support leaky modes. Benisty *et al.*[6] optimized a hybrid bottom-

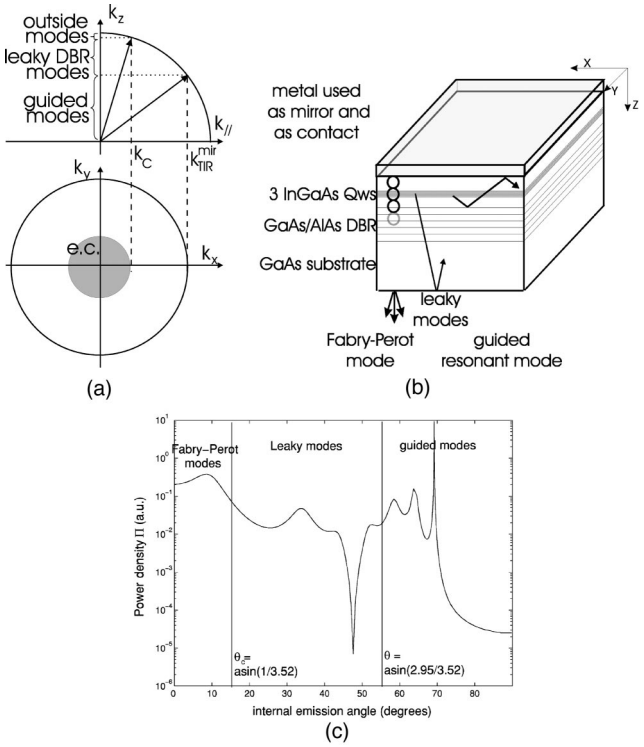

Fig. 1. (a) k-space presentation of outside, leaky, and guided modes, (b) RCLED, (c) typical internal angular emission distribution in RCLED, with $\theta = \arcsin(k_{\parallel}/k)$.

emitting cavity with a metallic and a DBR mirror for high extraction efficiency at 980 nm [Fig. 1(b)]. Figure 1(c) shows a simulation of the internal angular emission distribution with an indication of the fraction of the total emitted power in the respective modes [$\theta = \arcsin(k_{\|}/k)$]. The outside emission takes 20–25%. The power lost through the guided mode(s) accounts for 30–35%, through leaky DBR modes 25–35%, and through metallic absorption 10–15%. DBR modes cannot be avoided, but they can be minimized by using a higher-contrast DBR mirror, e.g., an AlOx/GaAs DBR.[8] The guided modes can be cut off by using a thinner cavity. However, the power of the latter will be divided over all modes, including the leaky DBR modes, resulting in only marginal extra power in the extractable Fabry–Perot mode, and most of the power (70%) will be absorbed in the substrate.[20] Since the integration of a more complex doping profile is more accessible in thicker cavities, a thicker cavity supporting the guided mode is to be preferred in electrically pumped devices.

B. Extraction of In-Plane Propagating Waves by Means of a Grating

Passive waveguide structures with grating couplers have been widely studied.[21–23] A guided mode propagating in a lossless planar waveguide structure equipped with a shallow lossless grating with appropriate period(s) $\mathbf{\Lambda}_i$ ($i = x, y'$) and resulting Bragg vector(s) $\mathbf{K}_i = 2\pi \mathbf{1}_{\Lambda_i}/\Lambda_i$ [see Figs. 2(a) and 2(d)] can be diffracted entirely toward the extraction cone. This can be easily illustrated by using a wave-vector presentation in the k space [$(\mathbf{k}_x, \mathbf{k}_y, \mathbf{k}_z) = (\mathbf{k}_{\|}, \mathbf{k}_z)$] (Fig. 2). This is called the wave-vector diagram (WVD).[13] Monochromatic light with frequency ν and vacuum wavelength $\lambda_0 = c/\nu$ and wave number $k_0 = 2\pi/\lambda_0$ is considered, with c the velocity of light. In the $\mathbf{k}_{\|}$ plane, the guided mode in the high-refractive-index waveguide (for GaAs $n \approx 3.52$) can be represented by its propagation constant $\beta = |\mathbf{k}_{\|}| = |\mathbf{k}_{0\|}| n_{\text{eff}}$ for azimuthal angle ϕ, $0 \leqslant \phi < 2\pi$, and n_{eff} is the effective refractive index of the guided mode. This leads to a circle in the WVD. Waves with in-plane k vector $\mathbf{k}_{\|}$ smaller than $2\pi/\lambda_0$ can escape the waveguide in a nonlateral way. This region of extractable waves is represented in the $\mathbf{k}_{\|}$ plane by the extraction cone ec, corresponding to ec, disk, $|\mathbf{k}_{\|}| < 2\pi n/\lambda_0$. Since the propagation constant β does not overlap the extraction cone, the guided wave will not be extracted out of the high-refractive-index slab (leaving evanescent coupling aside). However, when the interface of the slab is corrugated with a shallow grating, weakly affecting the propagation constant of the guided wave, waves with $\mathbf{k}_{\|} = \mathbf{k}_{0\|} n_{\text{eff}} + v\mathbf{K}_x + w\mathbf{K}_{y'}$, v, w integer, will be present according the Floquet–Bloch theorem. The guided mode will continuously couple power to these diffracted waves and vice versa. This can be represented in the WVD by a projection of the "guided" wave, represented in the WVD by the circle with radius β, toward the extraction cone along the Bragg vector. The overlapping part of the diffracted wave with the extraction cone can escape the waveguide. Thus the guided mode will leak power toward the extraction cone by means of diffracted waves. The appropriate period and lattice structure of the grating to maximize overlap depend on the dielectric-constant differences among the core, cladding, and vacuum. With a 1D grating and a waveguide configuration representative of GaAs RCLEDs, up to 22% of the diffracted guided wave overlaps the extraction cone [marked bold in Fig. 2(b)]. This 22% represents a maximum of the extractable fraction of the guided wave in this configuration. This can alternatively be represented graphically by a translation of the extraction cone toward the guided wave [Fig. 2(c)] instead of the translation of the circle that represents the guided wave toward the extraction-cone disk. The overlap of the guided mode and the translated extraction cone again represents an upper limit of the extraction efficiency. A 2D grating increases the extraction efficiency of the guided wave to 66% with a first-order grating (the guided mode is coupled toward the extraction cone through first-order diffraction) [Fig. 2(e)] and to 100% with a second-order grating (the guided mode is coupled toward the extraction cone through second-order diffraction) [Fig. 2(f)].

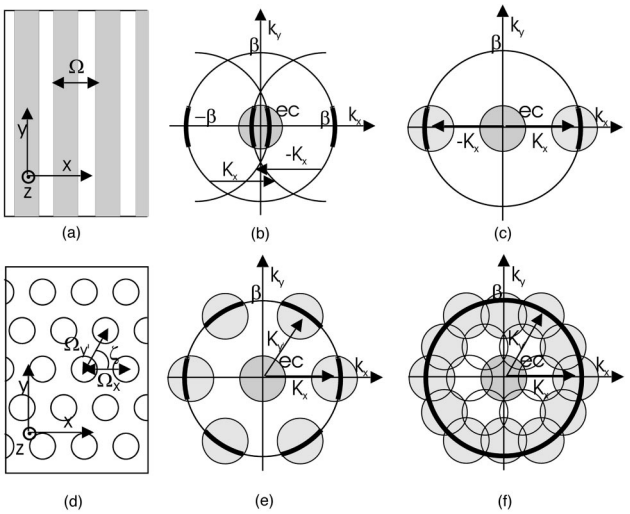

Fig. 2. Wave-vector diagram. (a) Top view of a 1D grating. (b) Extraction of guided mode with use of a 1D first-order grating ($\beta = |\mathbf{K}_x|$) presented in the $\mathbf{k}_{\|}$ plane: When the guided mode is projected toward the extraction cone, ec, the overlap of the diffracted light and the extraction cone can be extracted. This corresponds to a fraction of 22% of the guided mode. (c) Alternative graphic presentation to calculate the upper limit: projection of the extraction cone toward the guided mode by the Bragg vector. The overlap of the projected cone and the guided mode is limited to 22%. (d) Top view of a 2D grating ($\beta = |\mathbf{K}_i|$, $i = x, y'$). (e) Analog graphic presentation for a 2D first-order grating. (f) 2D second-order grating ($\beta = 2|\mathbf{K}_i|$).

It is worth emphasizing that this graphic analysis indicates qualitatively to what extent a grating structure can extract an in-plane guided mode. It only represents an upper limit of the extractable fraction of the guided wave. Quantitative information, e.g., the fraction of photons in the respective modes or absorption losses, has to be found by a rigorous analysis (see Section 3).

C. Grating-Assisted Resonant-Cavity LED

In a way similar to the extraction of a guided wave from a corrugated passive waveguide, the guided mode excited by a dipole placed inside a periodically corrugated layer structure can escape the cavity when the period, depth,

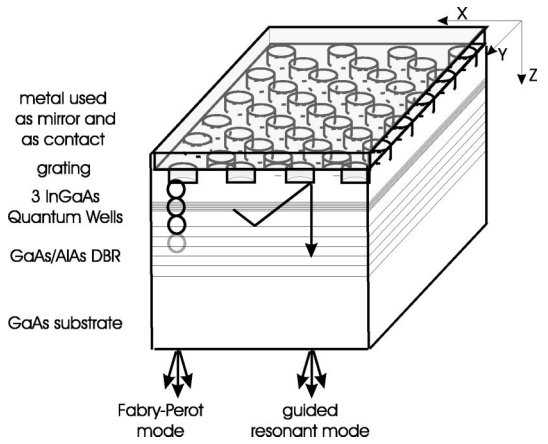

Fig. 3. Sketch of a GA-RCLED.

filling factor, lattice structure of the grating, and cavity thickness are chosen appropriately.

In the case of monomodal thin-film devices, the guided mode can be directly extracted.[13]

With use of a hybrid bottom-emitting cavity with metallic and DBR mirrors sustaining an extractable Fabry–Perot mode, guided mode(s) and leaky DBR modes, the grating will couple the guided mode to the extractable Fabry–Perot mode and vice versa. If the extractable resonant surface-normal mode has a lower Q factor than the nonextractable high-Q guided mode, reciprocal coupling of power between the resonant systems will result in a net power flow from the guided mode to the extraction cone in the case of negligible absorptions. The conceptual design of a GA-RCLED is depicted in Fig. 3.

3. THEORETICAL FORMULATION

A. Electric Dipole Emission in a Two-Dimensional Periodically Corrugated Multilayered Structure

The plane-wave matrix formalism for dipole radiation in a multilayer planar system[12] has been extended to calculate emission modification of a dipole placed in an arbitrary 2D periodically corrugated multilayered structure. The plane-wave matrix formalism is based on the Fourier transform with respect to x and y of the electromagnetic field emitted by an electrical dipole. The $k_\parallel$ Fourier spectrum contains arbitrarily large wave vectors k_x and k_y. Letting these plane propagative and evanescent waves propagate through the periodically corrugated multilayer permits the outside far-field radiated power to be calculated. This formalism is presented in this section.

The electromagnetic field $\mathbf{e}(x, y, z)$ [time dependence $\exp(-i\omega t)$ is assumed] can be expressed in terms of its Fourier components $\mathbf{e}_F(\theta, \phi, z)$, the plane-wave amplitude per solid angle, or the mode density,

$$\mathbf{e}(x, y, z) = \left(\int_0^{\pi/2} + \int_{\pi/2+i0}^{\pi/2+i\infty} \right) \sin\theta \, \mathrm{d}\theta \times \int_0^{2\pi} \mathrm{d}\phi \mathbf{e}_F(\theta, \phi, z) \exp(i\mathbf{k}_\parallel \mathbf{r}), \quad (1)$$

or by using the Wronskian conversion and expressing $\mathbf{e}_F$ as a function of k_x and k_y:

$$\mathbf{e}(e, y, z) = \int_{-\infty}^{\infty} \int_{-\infty}^{\infty} \frac{\mathrm{d}k_x \mathrm{d}k_y}{n k_0 k_z} \mathbf{e}_F(k_x, k_y, z) \times \exp(ik_x x + ik_y y). \quad (2)$$

In the presence of a diffractive grating, waves are coupled with each other according to the Bragg condition. This means that a wave with in-plane wave vector $\mathbf{k}_\parallel^{\mathrm{in}} = \mathbf{k}_\parallel^{00}$ gives rise to waves with in-plane wave vector $\mathbf{k}_\parallel^{vw}$ and vice versa (Fig. 4),

$$\mathbf{k}_\parallel^{vw} = \mathbf{k}_\parallel^{\mathrm{in}} + v \frac{2\pi}{\Lambda_x} \mathbf{1}_x + w \frac{2\pi}{\Lambda_{y'}} \mathbf{1}_{y'}, \quad (3)$$

where Λ_x is the period along the x direction and $\Lambda_{y'}$ is the period along the y' direction with $\mathbf{1}_{y'} = \mathbf{1}_x \cos(\zeta) + \mathbf{1}_y \sin(\zeta)$ and v, w integer. This implies that if matrices are introduced to express coupling between the coupled Bragg diffracted waves, the infinite integrals of Eq. (1) can be reduced to a finite integration region in the k space, bounded by the respective Bragg vectors,

$$\mathbf{e}(x, y, z) = \int_0^{2\pi/\Lambda x} \int_0^{2\pi/\Lambda_{y'}} \frac{\mathrm{d}k_x \mathrm{d}k_{y'}}{n k_0 k_z} K_{xy} \cdot \mathbf{E}_F, \quad (4)$$

where $\mathbf{E}_F$ represents a $VW \times 1$ column matrix (V and W are the number of diffracted orders retained in the calculation for the respective periodic directions) and K_{xy} is a $1 \times VW$ row matrix with elements

$$\mathbf{E}_F[Wv + w] = \mathbf{e}_F(k_x^{vw}, k_y^{vw}, z),$$

$$K_{xy}[Wv + w] = \exp(ik_x^{vw} x + ik_y^{vw} y),$$

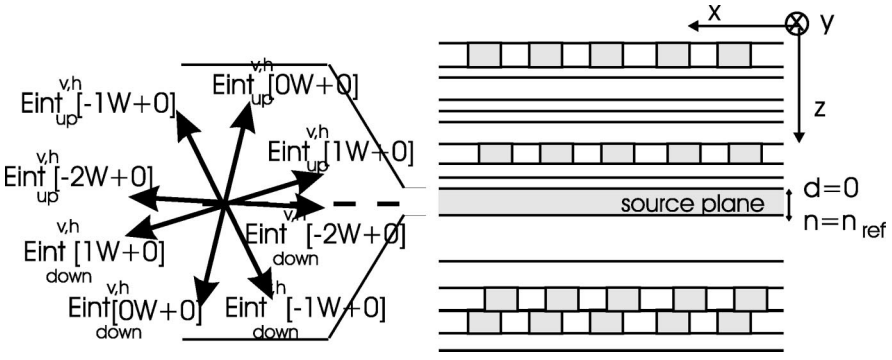

Fig. 4. Plane-wave formalism in a multilayer periodically corrugated structure. Eint is defined in Eq. (8).

$$k_x^{vw} = k_x^{00} + v\frac{2\pi}{\Lambda_x} + w\cos(\zeta)\frac{2\pi}{\Lambda_{y'}},$$

$$k_y^{vw} = k_y^{00} + w\sin(\zeta)\frac{2\pi}{\Lambda_{y'}},$$

$$0 \leqslant v < V,\ 0 \leqslant w < W,\ v \text{ and } w \text{ integer.} \quad (5)$$

In the presence of an absorbing medium located close to the emitter, the numbers of diffracted orders V and W retained in the calculation for the respective periodic directions have to be high enough to ensure inclusion of evanescent waves coupling to surface plasmons in this absorbing medium. Evanescent coupling to high-refractive-index layers is circumvented by letting the emission take place in a reference layer with zero thickness and $n_{\mathrm{ref}} > n_{\max}$, where n_{ref} is the refractive index of the reference source layer and $n_{\max}$ is the highest refractive index of the layer structure.

This reduction of the integration space to the Bragg unit cell in Eq. (4) implies that the plane-wave matrix formalism for homogeneous multilayer structures[6] can easily be extended when the electromagnetic field components and the reflection and transmission coefficients are replaced by matrices representative of the coupled waves that satisfy the Bragg condition. When this is done, the normalized (with respect to total emission in bulk media) source terms that are introduced in the plane-wave matrix formalism as an additive discontinuity across the dipole layer become column matrices of order $VW \times 1$. Table 1 summarizes the source terms A of the three configurations of dipole radiation that can be considered: (1) a vertical dipole v, radiating TM (p) waves; (2) a horizontal dipole h, radiating TM waves, averaged over the azimuthal angle of the dipole orientation; and (3) a horizontal dipole h, radiating TE (s) waves, averaged over the azimuthal angle of the dipole orientation.

The vectorial electric field $\mathbf{E}_F$ can be split into a TE part ($E^s = \mathbf{E}_F \cdot \|\mathbf{1}_k \times \mathbf{1}_z\|$) and a TM part ($E^p = \mathbf{E}_F \cdot \|\mathbf{1}_k \times (\mathbf{1}_k \times \mathbf{1}_z)\|$). Then $E^{h/v}$ stands for the $2VW \times 1$ matrix consisting of both the TE and the TM contributions resulting from horizontal or vertical dipoles, respectively. A similar notation is introduced for the dipole terms:

Table 1. Source Terms for Horizontal and Vertical Dipoles

Dipole	TE	TM
Horizontal	$A_{\uparrow\downarrow}^{h,s}[Wv + w] = \sqrt{\frac{3}{16\pi}}$	$A_{\uparrow\downarrow}^{h,p}[Wv + w] = \sqrt{\frac{3}{16\pi}}\frac{k_{z,vw}}{k}$
Vertical	$A_{\uparrow\downarrow}^{v,s}[Wv + w] = 0$	$A_{\uparrow\downarrow}^{v,p}[Wv + w] = \pm\sqrt{\frac{3}{8\pi}}\frac{k_{\parallel,vw}}{k}$

$$E^{h/v} = \begin{bmatrix} E^{h/v,s} \\ E^{h/v,p} \end{bmatrix},$$

$$E^{h/v}[Wv_2 + w] = \left(1 - \left\lfloor\frac{v_2}{V}\right\rfloor\right)E^{h/v,s}[Wv_2 + w] + \left\lfloor\frac{v_2}{V}\right\rfloor E^{h/v,p}[W(v_2 - V) + w],$$

$$0 \leqslant v_2 < 2V,\ 0 \leqslant w < W, \quad (6)$$

$$A_{\uparrow\downarrow}^{h/v} = \begin{bmatrix} A_{\uparrow\downarrow}^{h/v,s} \\ A_{\uparrow\downarrow}^{h/v,p} \end{bmatrix}, \quad (7)$$

where $\lfloor\rfloor$ means largest integer smaller than the argument. Calculating the electric field matrix caused by dipole emission in the direction corresponding to the (v_2, w) diffraction order then takes into account coupling between the respective polarizations. After accounting for the multiple reflections at the mirrors, we can write the upward- and downward-propagating extracted fields as[15]

$$E_{\mathrm{up}}^{h/v}(v_2, w) = \frac{T_{\mathrm{up}}(R_{\mathrm{down}}SE_{v_2w}A_{\downarrow}^{h/v} - SE_{v_2w}A_{\uparrow}^{h/v})}{I - R_{\mathrm{down}}R_{\mathrm{up}}} = T_{\mathrm{up}}E\mathrm{int}_{\mathrm{up}}^{h/v},$$

$$E_{\mathrm{down}}^{h/v}(v_2, w) = \frac{T_{\mathrm{down}}(R_{\mathrm{up}}SE_{v_2w}A_{\uparrow}^{h/v} - SE_{v_2w}A_{\downarrow}^{h/v})}{I - R_{\mathrm{down}}R_{\mathrm{up}}} = T_{\mathrm{down}}E\mathrm{int}_{\mathrm{down}}^{h/v}, \quad (8)$$

with I the $2VW \times 2VW$ unity matrix and R_{up}, T_{up}, R_{down} and T_{down} the $2VW \times 2VW$ reflection and transmission matrices, respectively, of the multilayer on top of and below the active layer. In these matrices the element $[Wv_2 + w, Wv_2' + w']$ relates the (v_2', w') diffracted order to the (v_2, w) wave. Calculation of these matrices will be discussed in the Subsection 3.B. SE_{v_2w} is a $2VW \times 2VW$ matrix with all elements zero but the (v_2, w)th element equal to 1, making the dipole emission active only in the direction corresponding to the (v_2, w) diffraction order. $E\mathrm{int}$ represents the internal electric field matrix (see Fig. 4).

B. Calculation of R and T

To calculate the reflection and transmission matrices of the periodically corrugated multilayers, a rigorous electromagnetic analysis is needed with respect to the sensitivity of the cavity behavior to phase and amplitude shifts of the cavity mirror's reflection coefficients. We have implemented the rigorous coupled-wave analysis for gratings proposed by Moharam *et al.*[24,25] and reformulated by Li[26] and Lalanne[27] to improve TM convergence. It is a straightforward, noniterative, deterministic technique, based on a state-variables representation of the coupled-wave amplitudes of the space-harmonic fields, permitting calculation of the field in terms of eigenfunctions and eigenvectors of the coefficient matrix defined by the coupled-wave equations. The coupled-wave equations are Maxwell's equations solved in the grating layers for

the field's spatial Fourier expansion. The accuracy of the obtained solution depends solely on the number of terms retained in the space-harmonic expansion of the field, with conservation of energy always retained. For a detailed discussion on the rigorous coupled-wave analysis, the reader is referred to Refs. 24–27.

C. Extraction Efficiency

The extraction efficiency can be found by integrating the normalized power of the outside plane waves per unit solid angle and per unit surface over the desired solid angle. This normalized power density can be calculated from Eqs. (8), which expresses the plane-wave amplitude of the electromagnetic field per unit solid angle as a function of the normalized source terms. However, calculation of the inside and outside power flux normalized to the source power flux must take into account both the solid angle transformation due to refraction and the solid angle transformation due to diffraction (Fig. 5).

At a 2D periodically corrugated interface, the normalized active transmitted (reflected) power per unit interface area t_{pow}^{vw} (r_{pow}^{vw}) of the $(Wv + w)$th diffracted order or, equally, the amplitude ratio of the projection onto the z axis of the real transmitted (reflected) Poynting vector $\mathbf{s}^{vw}$ to the real incident Poynting vector $\mathbf{s}^{\mathrm{in}}$, can be written as function of the field amplitudes $\mathbf{t}_f^{vw}(\mathbf{r}_f^{vw})$:

$$\begin{aligned}
\mathrm{Re}(s \cdot \mathbf{1}_z) &= \frac{1}{2}\mathrm{Re}(\mathbf{e} \times \mathbf{h}^*) \cdot \mathbf{1}_z, \\
\mathrm{Re}(s_z^{\mathrm{in}}) &= \frac{1}{2}\frac{\mathrm{Re}(k_z^{\mathrm{in}})}{\omega\mu_0}, \\
\mathrm{Re}(s_z^{vw}) &= \frac{1}{2}\frac{\mathrm{Re}(k_z^{vw})}{w\mu_0}\mathbf{t}_f^{vw}\mathbf{t}_f^{vw*}, \\
t_{\mathrm{pow}}^{vw} &= \frac{\mathrm{Re}(s_z^{vw})}{\mathrm{Re}(s_z^{\mathrm{in}})},
\end{aligned} \tag{9}$$

or with t_{sf}^{vw}, t_{pf}^{vw} the components of the electric and magnetic field vectors representing TE and TM polarizations:

$$t_{\mathrm{pow}}^{vw} = |t_{s\,f}^{vw}|^2\,\mathrm{Re}\left(\frac{k_z^{vw}}{k_z^{\mathrm{in}}}\right) + |t_{p\,f}^{vw}|^2\,\mathrm{Re}\left(\frac{k_z^{vw}/n_{\mathrm{sur}}^2}{k_z^{\mathrm{in}}}\right). \tag{10}$$

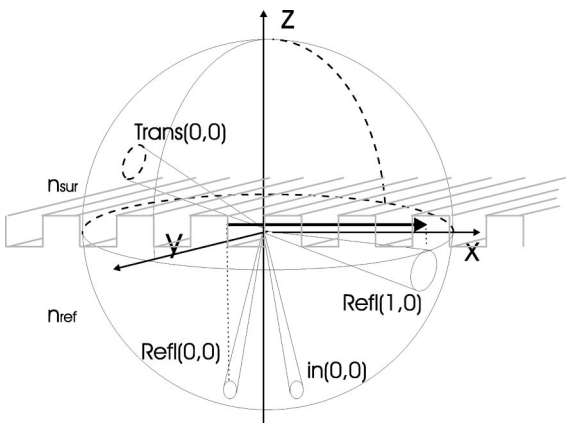

Fig. 5. Solid-angle transformation due to refraction and diffraction.

Taking into account Eqs. (9) and (10), we can calculate a Π_Ω matrix from Eq. (8):

$$\begin{aligned}
\Pi_\Omega^s[Wv + w] &= \Sigma_{v_2',w'}^{2V,W}|E^{h/v,s}(v_2', w)[Wv + w]|^2 \\
&\quad \times \mathrm{Re}\left(\frac{k_z^{vw}}{k_z^{v_2',w'}}\frac{1}{n_{\mathrm{ref}}k_0k_z^{v_2'w'}}\right), \\
\Pi_\Omega^p[Wv + w] &= \Sigma_{v_2',w'}^{2V,W}|E^{h/v,p}(v_2', w')[Wv + w]|^2 \\
&\quad \times \mathrm{Re}\left(\frac{k_z^{vw}/n_{\mathrm{sur}}^2}{k_z^{v_2',w'}}\frac{1}{n_{\mathrm{ref}}k_0k_z^{v_2'w'}}\right),
\end{aligned} \tag{11}$$

with $\Pi_\Omega^{s,p}[Wv + w]$ the normalized power per unit spatial frequency in a direction corresponding to $\mathbf{k}^{vw}$. Finally, the normalized power per unit surface can be calculated by integrating the matrix product over the Bragg unit cell:

$$p^{s,p} = \int_0^{2\pi/\Lambda_x}\int_0^{2\pi/\Lambda_{y'}} \mathrm{d}k_x\mathrm{d}k_{y'}I_r\Pi_\Omega^{s,p}, \tag{12}$$

with I_r a unity $1 \times VW$ row matrix. This normalized power defines the measure for extraction efficiency when the ratio of the outside power to the total power is considered.

Numerical calculation of the integral in the formula of the normalized power [Eq. (12)] can be done by discretization of the integrand. This discretization has to be done with care, because the power density function Π_Ω will show narrow peaks around multiple-beam interference effects (e.g., the extracted guided wave). A locally narrower grid will then be required around these narrow modes.

D. Importance of Dipole Position: Remark on Eqs. (11)

In the case of a set of $\mathbf{k}_\parallel$ vectors coupled by the Bragg condition, the contributions of the source terms of the respective emission directions to a specific spatial frequency $\mathbf{k}_\parallel^{pq}$ of this set are considered to interact incoherently. Although the respective contributions of a single dipole at a specific location to a certain diffraction order do interact coherently, the dependency of the intensity on the dipole, position is averaged out when all dipole positions are considered in a Bragg unit cell. This incoherent interaction of the respective contributions of a single dipole used to calculate the normalized power per unit spatial frequency Π_Ω in Eq. (11), is justified by the fact that the phase of the reflection coefficients $R_{vw\to pq}$ depends on the in-plane position of the dipole. This phase-shift variation as a function of the position of the emitter is proportional to $\mathbf{k}_\parallel^{pq} - \mathbf{k}_\parallel^{vw} = (p - v) \times (2\pi/\Lambda_x)\mathbf{1}_x + (q - w)(2\pi/\Lambda_{y'})\mathbf{1}_{y'}$ and thus shows a proportional periodicity. Considering dipole emission intensity over a periodic unit cell will average out this phase-shift variation, resulting in an incoherent interaction of the distinct Bragg coupled contributions with a single spatial frequency.

4. NUMERICAL RESULTS

A. Grating-Assisted Resonant-Cavity LEDs with Use of a One-Dimensional Grating

One-dimensional gratings used in RCLEDs do not help much to boost the efficiency, as shown graphically above, but they do give rise to an asymmetric, polarization-selective emission. This polarization is not related to the polarizations as defined for the dipole emission in Section 3 but defines the orientation of the electric field $\mathbf{E}$ with respect to the Bragg vector $\mathbf{K}_\Lambda$ of the 1D grating. TE refers to an in-plane $\mathbf{E}$ component normal to $\mathbf{K}_\Lambda$. Figure 6 shows the polarization-selective behavior of a hybrid bottom-emitting cavity with a metallic/semiconductor 1D grating as top mirror and a GaAs/AlAs DBR as bottom mirror. The period of the grating is 600 nm (second-order grating), the depth is 100 nm, and the filling factor is 0.3. The surface-normal emission shows clearly a polarization-selective emission preferentially in the TE polarization.

Figure 7 shows the angle-resolved spectrum for TE emission in the plane containing the Bragg vector and $\mathbf{k}_z$ (azimuthal angle $\phi = 0$). According to the WDM, quasi-guided modes are extracted into an angle θ_{out} corresponding to $\mathbf{k}_\parallel^{\text{out}}$ when their in-plane wave vector $\mathbf{k}_\parallel^{gm}$ satisfies the Bragg condition: $\mathbf{k}_\parallel^{gm} = \mathbf{k}_\parallel^{\text{out}} \pm v\mathbf{K}_\Lambda$. This condition is fulfilled by two counterpropagating modes when $v = 2$ (second-order grating), resulting in a splitting of the angle-resolved spectrum when oblique angles are considered ($\phi = 0$).

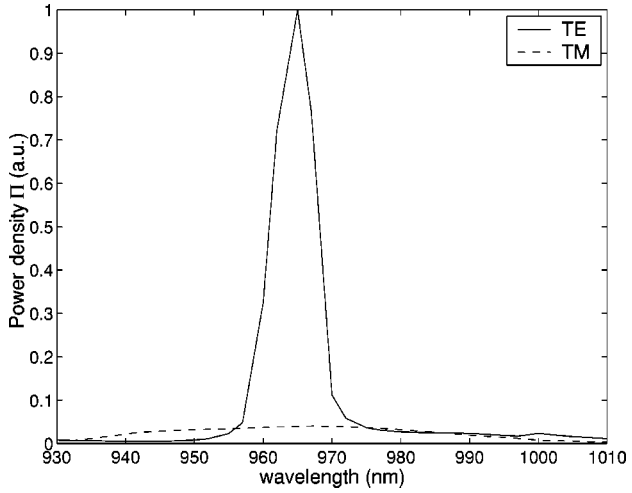

Fig. 6. Polarization-selective emission: surface-normal spectral data for TE and TM polarization.

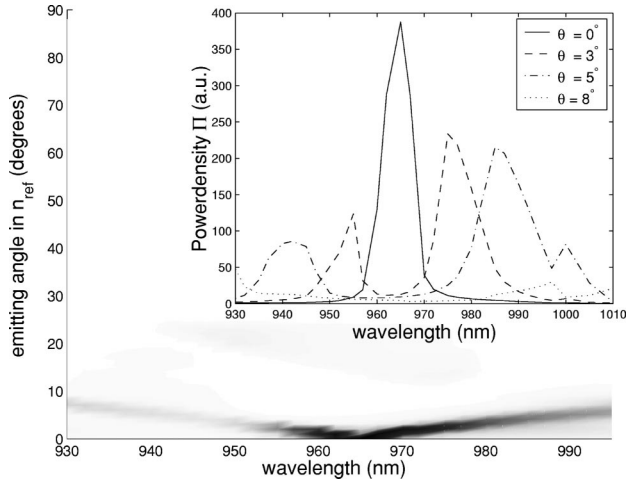

Fig. 7. Angle-resolved spectrum in the plane mounted by the Bragg vector and $\mathbf{k}_z$ (azimuthal angle $\phi = 0$).

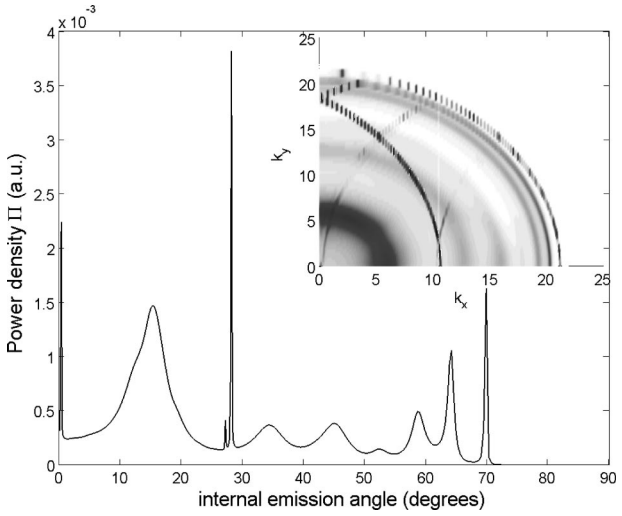

Fig. 8. Simulated power per unit solid angle along the x axis as a function of the angle in the highest-index medium. Inset: contour plot of the simulated power per unit solid angle in $\mathbf{k}_\parallel$ space.

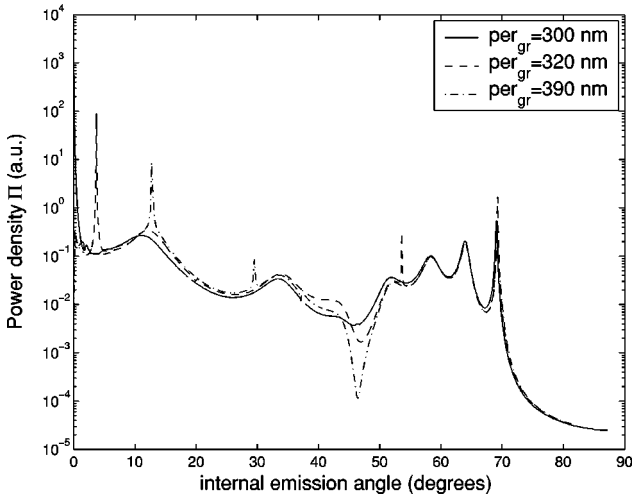

Fig. 9. Simulated power per unit solid angle along the x axis as a function of the angle for increasing period.

The downward power per unit solid angle for a monochromatic source as a function of the angle in the highest-index medium along the x axis is plotted for this device in Fig. 8. Diffraction of the guided wave toward the outside mode is clearly visible when this plot is compared with the corresponding plot of a homogeneous layered RCLED in Fig. 1(c). On top of the lower Q-factored Fabry–Perot mode (10°–20°), two sharp peaks corresponding to the first and second diffraction orders can be distinguished at 0.1° and 27°, respectively. The inset of Fig. 8 shows the respective contour plot in the $\mathbf{k}_\parallel$ space. The WVD of Fig. 2(b) can be distinguished. The speckled character of the diffracted waves in this contour plot is attributed to the finite grid.

With increasing period of the grating, the peak corresponding to the extractable diffracted guided wave will shift toward larger angles. This is shown in Fig. 9 for a first-order grating with periods 300, 320, and 390 nm. In the WVD this corresponds to projection of the guided-wave circle toward the extraction cone by use of a Bragg vector with decreasing length. The simulations are in correspondence with previously published experimental results.[28]

B. Grating-Assisted Resonant-Cavity LEDs with Use of a Two-Dimensional Grating

The downward power per unit solid angle as a function of the angle in the highest-index medium for a hybrid

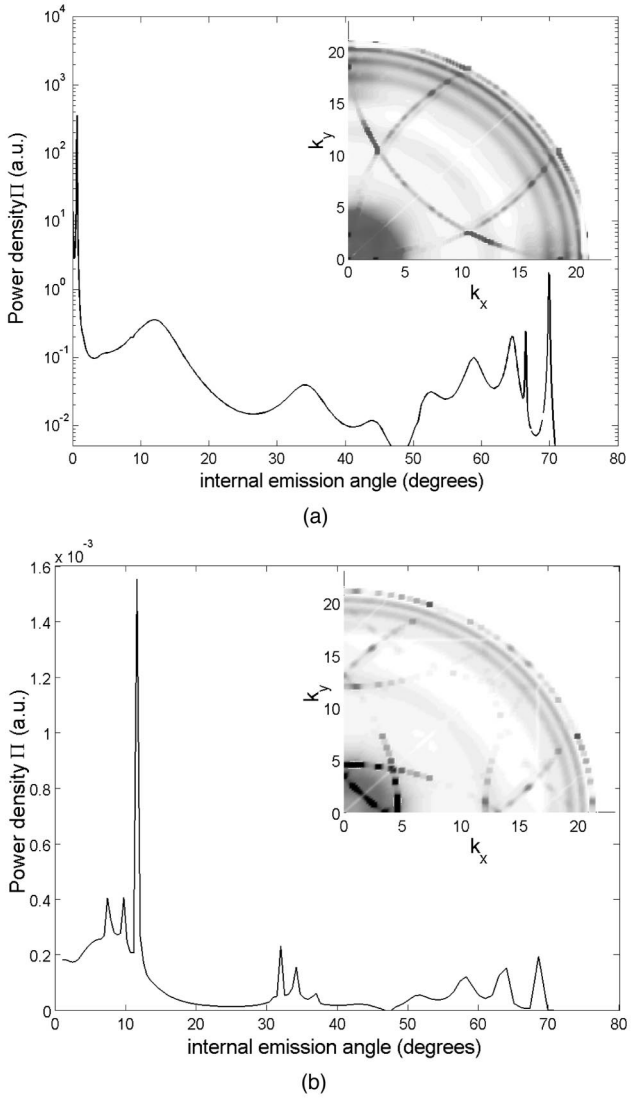

Fig. 10. Simulated power per unit solid angle along the x axis as a function of the angle in the highest-index medium. Inset: contour plot of the simulated power per unit solid angle in $\mathbf{k}_{\parallel}$ space. (a) 2D partially metallized air–semiconductor square lattice grating of depth 90 nm, fill factor 0.5, and period 300 nm; (b) 2D partially metallized air–semiconductor square lattice grating of depth 90 nm, fill factor 0.5, and period 390 nm.

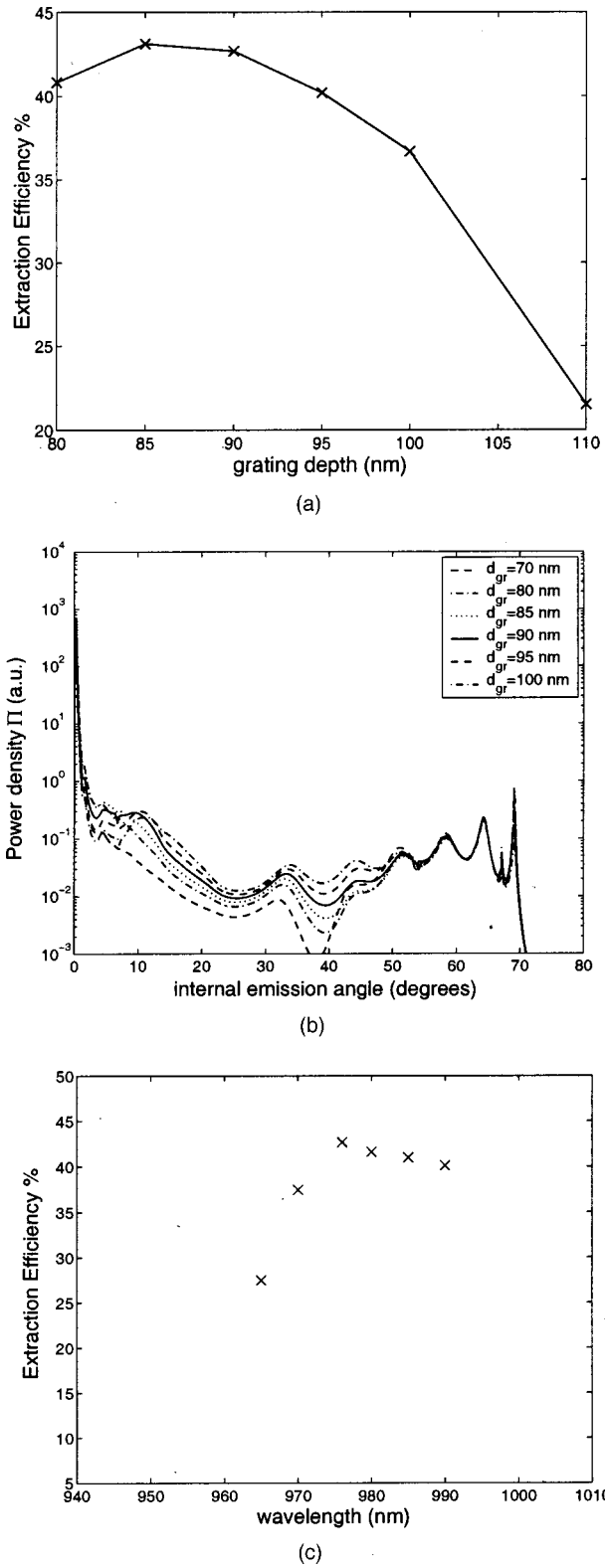

Fig. 11. (a) Extraction efficiency of a hybrid bottom-emitting cavity with a 2D partially metallized air–semiconductor square lattice grating with period 300 nm and wavelength 976 nm as a function of the grating depth, (b) corresponding power per unit solid angle along the x axis as a function of the angle in the highest-index medium, (c) extraction efficiency for a grating with depth 90 nm as a function of the emitted wavelength.

bottom-emitting cavity is plotted in Fig. 10. The data in Fig. 10(a) are representative for a grating period of 300 nm and depth 90 nm; Fig. 10(b) is representative for a grating period of 390 nm and depth 90 nm. The 2D square lattice grating is partially covered with metal; this corresponds to obliquely evaporating the metallic contact on the grating that covers only the grating teeth. In contrast to full metallic gratings, the metallic absorption of partially metallized gratings is reduced, while homogeneous current injection remains. The inset is the respective representation in the $\mathbf{k}_{\|}$ space. The diffracted guided wave is clearly present at extractable angles when the period is chosen to be 300 nm. When the period is increased, the peak corresponding the diffracted guided mode shifts to larger angles. This is similar to the case of GA-RCLEDs with a 1D grating.

The device can be optimized for high brightness by choosing the right combination of parameters: grating depth, grating period, filling factor, lattice structure, grating materials, cavity thickness, position of QWs, reflectivity of the bottom mirror, etc. As an example, the dependence on grating thickness for a hybrid bottom-emitting cavity with a 2D air–semiconductor square lattice grating of period 300 nm and filling factor 0.5 is shown in Fig. 11(a). The 2D grating is partially covered with metal. Figures 11(a) and 11(c) plot the extraction efficiency as a function of the grating depth, with a monochromatic source. Plots of the corresponding downward power per unit solid angle as a function of the angle show not only that the diffractive properties of the grating affect the extraction efficiency but also that the cavity tuning along the z axis plays a role in the brightness of the device [Fig. 11(b)]. The tuning affects the round-trip condition, which in turn influences the extractable Fabry–Perot mode. The equivalent phase plane of the grating (an imaginary plane that shows equivalent phase conditions for the zeroth-order reflection at the grating) varies with the depth of the grating. A deeper grating corresponds to a shorter cavity. Extraction of the Fabry–Perot mode is most efficient when the cavity is slightly detuned toward thicker cavities.[20]

A local optimum of more than 43% has been found with partial scanning of the large parameter space. Although this percentage holds only for monochromatic sources, the GA-RCLED is promising for highly efficient devices with finite intrinsic spectra, as can be seen in Fig. 11(c). The efficiency remains high over a wavelength range of 970–990 nm. This range overlaps the intrinsic spectrum of the considered devices (FWHM = 20 nm).

5. CONCLUSION

A design for high-brightness RCLEDs was presented. An electromagnetic analysis for dipole emission in periodically corrugated multilayered systems was detailed. Implementation of this method is straightforward. Numerical calculations for a hybrid bottom-emitting cavity with a DBR bottom mirror and a partially metallic covered 2D air–semiconductor grating show that efficiencies of 40% can be obtained.

ACKNOWLEDGMENTS

Danaë Delbeke thanks the Institute for the Promotion of Innovation by Science and Technology (IWT) in Flanders for financial support. This research was developed in the framework of the European Union Esprit research program SMILED (Semiconductor Microcavity Light Emitting Diodes) and the Belgian Inter-University Attraction Pole IAP IV-13.

Corresponding author Danaë Delbeke can be reached by e-mail at danae.delbeke@intec.rug.ac.be

REFERENCES

1. K. Gillessen and W. Schairer, *Light Emitting Diodes: an Introduction*, (Prentice-Hall International, Cambridge, UK, 1987).
2. W. Schmid, F. Eberhard, R. Jäger, R. King, M. Miller, J. Joos, and K. J. Ebeling, "45% quantum efficiency light-emitting diodes with radial outcoupling taper," in *Light-Emitting Diodes: Research, Manufacturing, and Applications IV*, H. W. Yao, I. T. Ferguson, and E. F. Schubert, eds., Proc. SPIE **3938**, 90–97 (2000).
3. M. O. Holcomb, M. R. Krames, G. E. Hofler, C. Carter-Coman, E. Chen, P. Grillot, K. Park, N. F. Gardner, J.-W. Huang, J. Posselt, D. Collins, S. A. Stockman, G. M. Craford, F. A. Kish, I.-H. Tan, T. S. Tan, C. P. Kocot, and M. Hueschen, "High power truncated-inverted-pyramid $(Al_xGa_{1-x})_{0.5}In_{0.5}P$ light-emitting diodes exhibiting >50% external quantum efficiency," Appl. Phys. Lett. **75**, 9365–9367 (1993).
4. I. Schnitzer, E. Yablonovitch, C. Carneau, T. J. Gmitter, and A. Scherer, "30% external quantum efficiency from surface textured, thin-film light-emitting diodes," Appl. Phys. Lett. **63**, 2174–2176 (1993).
5. R. Windisch, C. Rooman, S. Meinlschmidt, P. Kiesel, D. Zipperer, G. H. Doehler, B. Dutta, M. Kuijk, G. Borghs, and P. Heremans, "Impact of texture-enhanced transmission on high-effiency surface-textured light-emitting diodes," Appl. Phys. Lett. **79**, 2315–2317 (2001).
6. H. Benisty, H. De Neve, and C. Weisbuch, "Impact of planar microcavity effects on light extraction—part I: basic concepts and analytical trends," IEEE J. Quantum Electron. **34**, 1612–1631 (1998).
7. H. Benisty, H. De Neve, and C. Weisbuch, "Impact of planar microcavity effects on light extraction—part II: selected exact simulations and role of photon recycling," IEEE J. Quantum Electron. **34**, 1632–1643 (1998).
8. J. J. Wierer, D. A. Kellogg, and N. Holonyak, "Tunnel contact junction native-oxide aperture and mirror vertical-cavity surface-emitting lasers and resonant-cavity light-emitting diodes," Appl. Phys. Lett. **74**, 926–928 (1999).
9. I. Schnitzer, E. Yablonovitch, C. Caneau, and T. J. Gmitter, "Ultrahigh spontaneous emission quantum efficiency, 99.7% internally and 72% externally, from AlGaAs/GaAs/AlGaAs double heterostructures," Appl. Phys. Lett. **62**, 131–133 (1993).
10. M. G. Salt, P. Andrew, and W. L. Barnes, "Microcavities, texture symmetry, and photonic bandgaps," J. Opt. Soc. Am. B **18**, 240–243 (2001).
11. S. C. Kitson, W. L. Barnes, and J. R. Sambles, "Photonic bandgaps in metallic microcavities," J. Appl. Phys. **84**, 2399–2403 (1998).
12. M. G. Salt and W. L. Barnes, "Flat photonic bands in guided modes of textured metallic microcavities," Phys. Rev. B **61**, 11125–11135 (2000).
13. H. Rigneault, F. Lemarchand, A. Sentenac, and H. Giovannini, "Extraction of light from source located inside waveguide grating structures," Opt. Lett. **24**, 148–150 (1999).

14. J. M. Lupton, B. J. Matterson, I. D. W. Samuel, M. J. Jory, and W. L. Barnes, "Bragg scattering from periodically microstructured light emitting diodes," Appl. Phys. Lett. **77**, 3340–3342 (2000).
15. D. Delbeke, B. Dhoedt, R. Bockstaele, I. Moerman, P. Van Daele, T. F. Krauss, and R. Baets, "Electrically pumped photonic crystal micro-cavity light emitting diodes," in *Proceedings of IEEE/LEOS Summer Topical Meetings* (Institute of Electrical and Electronics Engineers, New York, 1999), pp. 71–72.
16. A. A. Erchak, D. J. Ripin, S. Fan, P. Rakich, J. D. Joannopoulos, E. P. Ippen, G. S. Petrich, and L. A. Kolodziejsk, "Enhanced coupling to vertical radiation using a two-dimensional photonic crystal in a semiconductor light-emitting diode," Appl. Phys. Lett. **78**, 563–565 (2001).
17. M. Rattier, H. Benisty, and C. Weisbuch, "Photonic crystal extractor," in *Electromagnetic Crystal Structures: Proceedings of Workshop on Photonic and Electromagnetic Crystal Structures III (PECS3)* (T. F. Krauss, University of St. Andrews, St. Andrews, UK, 2001).
18. M. Boroditsky, T. F. Krauss, R. Coccioli, R. Vrijen, R. Bhat, and E. Yablonovitch, "Light extraction from optically pumped light-emitting diode by thin-slab photonic crystal," Appl. Phys. Lett. **75**, 1036–1038 (1999).
19. H. Rigneault, F. Lemarchand, and A. Sentenac, "Dipole radiation into grating structures," J. Opt. Soc. Am. A **17**, 1048–1058 (2000).
20. H. De Neve, "Design and fabrication of light emitting diodes based on the microcavity effect," Ph. D. dissertation (Ghent University, Ghent, Belgium), p. 110 (1997).
21. E. G. Loewen and E. Popov, *Diffraction Gratings and Applications* (Marcel Dekker, New York, 1997).
22. S. Zhang and T. Tamir, "Rigorous theory of grating assisted couplers," J. Opt. Soc. Am. A **13**, 2403–2413 (1996).
23. N. H. Sun, J. K. Butler, G. A. Evans, L. Pang, and P. Congdon, "Analysis of grating-assisted directional couplers using the Floquet–Bloch theory," Appl. Phys. Lett. **13**, 2301–2315 (1997).
24. M. G. Moharam, E. B. Grann, D. A. Pommet, and T. K. Gaylord, "Formulation of stable and efficient implementation of the rigorous coupled-wave analysis of binary gratings," J. Opt. Soc. Am. A **12**, 1068–1076 (1995).
25. M. G. Moharam, D. A. Pommet, E. B. Grann, and T. K. Gaylord, "Stable implementation of the rigorous coupled-wave analysis for surface-relief gratings: enhanced transmittance matrix approach," J. Opt. Soc. Am. A **12**, 1077–1086 (1995).
26. L. Li, "Use of Fourier series in the analysis of discontinuous periodic structures," J. Opt. Soc. Am. A **13**, 1870–1876 (1996).
27. P. Lalanne, "Effective properties and band structures of lamellar subwavelength crystals: plane-wave method revisited," Phys. Rev. B **58**, 9801–9807 (1998).
28. D. Delbeke, K. Vandeputte, R. Baets, R. Bockstaele, B. Dhoedt, I. Moerman, P. Van Daele, and S. Verstuyft, "Holographically defined grating assisted micro-cavity light emitting diodes," in *Proceedings of the IEEE/LEOS Benelux Symposium* (Faculté Politechnique de Mons, Mons, Belgium, 1999), pp. 159–162.